Article

Graphene-Modified Electrode for Linear Sweep Voltammetric Sensing of Catechol

Florina Pogăcean, Lidia Măgeruşan *, Alexandru Turza and Stela Pruneanu *

National Institute for Research and Development of Isotopic and Molecular Technologies, 67-103 Donat Street, 400293 Cluj-Napoca, Romania; florina.pogacean@itim-cj.ro (F.P.); alexandru.turza@itim-cj.ro (A.T.)
* Correspondence: lidia.magerusan@itim-cj.ro (L.M.); stela.pruneanu@itim-cj.ro (S.P.)

Abstract: A graphene sample (EGr) was obtained in a single-step synthesis by electrochemical exfoliation of graphite rods. A combination of 0.05 M ammonium sulfate and 0.05 M ammonium thiocyanate was employed, leading to a graphene sample composed of few-layer, multi-layer and graphene oxide flakes. Due to the mild exfoliation conditions, large sheets with linear sizes in the range of tens to hundreds of micrometers were produced. The LSV technique gave information about the effect of catechol concentration on the electrochemical signal of bare and graphene-modified electrodes. Based on the resulting calibration plots, the corresponding analytical parameters (linear range, sensitivity, limit of quantification and limit of detection) were calculated for each electrode. In the case of the EGr/GC electrode the linear range was from 6×10^{-7} to 1×10^{-4} M catechol. The detection limit was low (1.82×10^{-7} M) while the quantification limit was 6×10^{-7} M. The sensitivity was five times higher than that corresponding to bare GC, proving the excellent electro-catalytic properties of the graphene-modified electrode. The practical applicability of the graphene-modified electrode was tested in tap water, obtaining an excellent recovery of 102%.

Keywords: catechol; graphene; modified electrodes; electrochemical detection; linear sweep voltammetry

1. Introduction

Catechol, a key dihydroxybenzene compound, also known as pyrocatechol ($C_6H_4(OH)_2$), naturally occurring at trace amounts in different plants (willow, pine, oak, beet sugar, onion, apple) was primarily identified in the destructive distillation of the plant extract catechin [1]. Currently, over 20 thousand tons of catechol are produced annually, employed mainly as common building blocks in the industrial production of agrochemicals/insecticides, different pharmaceuticals, fragrances and flavors [2]. Furthermore, due to its recognized antioxidant, anticorrosive and chelating properties catechol is massively employed in electroplating, in the dying and ink production industry, photography and organic synthesis [3]. Catechol is not present in the human body. However, human plasma contains different compounds including catechol units in their structure which are generally referred to as catechols [4]. Nowadays, different amounts of catechol may be spread into the environment with negative impacts on the human health. Excessive exposure to catechol can be harmful due to its reducing properties. Some laboratory investigations involving experimental animals have revealed its possible carcinogenicity [5–7]. Therefore, the development of sensitive, rapid and selective detection methods for catechol is of great importance. Electrochemical sensors have emerged as highly efficient tools for detecting

catechol, due to their inherent advantages of having a low cost, portability, and fast response times [8,9]. Multiple reports regarding concomitant catechol and hydroquinone electrochemical assays are provided by Chetankumar and his collaborators employing different modified electrodes: a voltammetric sensor based on a carbon paste electrode modified with direct green 6 [10]; a pencil graphite electrode modified with direct yellow 11 [11]; or a carbon paste electrode modified with a thin film of benzoguanamine [12]. A sensor for catechol and hydroquinone based on a poly-nile blue-modified glassy carbon electrode is also reported by Teradale et al. [13], while Dang and his collaborators achieved hydroquinone and catechol detection using the synergic effect of electropolymerized nicotinic acid film and a Cd-doped $ZnWO_4$ nanoneedle [14]. Zhao et al. developed a nickel oxide/carbon nanotube (NiO/CNT) nanocomposite–glassy carbon-modified electrode for the electrochemical sensing of hydroquinone and catechol [15]; a multi-walled carbon nanotubes/polydopamine/gold nanoparticles composite was employed as sensing layer by Wang Y. et al. [16], while Wang, J. et al., used a gold nanoparticle-decorated biochar-modified electrode [17]. However, selective and sensitive catechol electrochemical determination still remains a challenge. Among the various materials employed in sensor design, graphene stands out as a promising candidate. Graphene's extraordinary electrical conductivity, large surface area and chemical stability make it an ideal platform for electrochemical sensing applications [18–21].

In this study, we report on the development of a graphene-based electrochemical sensor for the detection of catechol using Linear Sweep Voltammetry (LSV). The aim of this work was to optimize the electrochemical performance of a glassy carbon electrode through surface modification with graphene-based material, investigate the newly developed sensitive layer detection capabilities and evaluate its potential for practical applications in environmental monitoring and related fields. The proposed method enables sensitive catechol detection providing clear and reliable signals.

2. Materials and Methods

2.1. Chemicals

The employed sodium acetate buffers were prepared from sodium acetate (CH_3COONa) (VWR Chemicals, Leuven, Belgium) and acetic acid (CH_3COOH) (Chemical Company, Iasi, Romania). The phosphate buffers were prepared from sodium phosphate monobasic (NaH_2PO_4) and sodium phosphate dibasic ($Na_2HPO_4 \cdot 12H_2O$), both from VWR Chemicals, Belgium. We used potassium ferrocyanide ($K_4[Fe(CN)_6]$) (Sigma-Aldrich, Sternheim, Germany), potassium chloride (KCl) (Sigma-Aldrich, Sternheim, Germany), potassium chloride (KCl, 99.999%, Merck, Darmstadt, Germany); sodium nitrite ($NaNO_2$) and sodium bicarbonate ($NaHCO_3$) were from J.T. Baker, Sternheim, Germany; catechol (C_6H_4–1,2-$(OH)_2$, ≥95.0%, Sigma-Aldrich, St. Louis, MO, USA), hydroquinone (C_6H_4–1,4-$(OH)_2$, ≥99%; Fluka Chemie GmbH, Buchs, Switzerland) resorcinol (C_6H_4–1,3-$(OH)_2$, ≥99%; Sigma-Aldrich, St. Louis, MO, USA) and dimethylformamide ($HCON(CH_3)_2$) (DMF; JT-Baker, HPLC grade, Sternheim, Germany) were also employed. All the electrolyte solutions were prepared with double-distilled water produced with Fistreem Cyclon equipment (Fistreem International Ltd., Cambridge, UK).

2.2. Electrochemical Exfoliation of Graphite Rods

The graphene sample (EGr) was synthesized by the electrochemical exfoliation of graphite rods via pulses of current in an aqueous solution (100 mL) containing specific salts, such as 0.05 M ammonium sulfate ($(NH_4)_2SO_4$) and 0.05 M ammonium thiocyanate (NH_4SCN). A bias of 9 V was applied between the graphite rods and the time parameters for the current pulses were set before starting the experiment: 0.8 s for the current pulse

duration and 0.2 s for the pause between two current pulses. After 4 h, the black powder deposited preponderantly around the anode was collected by decantation, washed with 10 L of distilled water and finally dispersed by ultrasound (30 min) in 125 mL water. Larger particles were removed from the suspension by filtering on a Whatman ashless cellulose filter paper—589/2, flat, Ø110 mm. The final step was the drying step, achieved by liophilization for 24 h, at $-90\ ^\circ$C and 0.004 bar.

2.3. Preparation of Graphene-Modified Electrode (EGr/GC)

The glassy carbon (GC) surface was polished on a piece of felt then covered by graphene previously suspended in N,N-dimethylformamide (DMF; 2 mg/mL). The graphene powder was dispersed by sonication for 3 min with a SONICS Vibra-Cell finger device. Next, on the bare GC surface a volume of 9 μL from the above dispersion was drop-casted and dried for 24 h at room temperature. The obtained modified electrode was denoted EGr/GC and then employed for catechol detection.

2.4. Instruments

Scanning Electron Microscopy (SEM) investigation of the graphene sample was performed with a Hitachi SU 8230 system (Hitachi High-Technologies Corp., Ibaraki, Japan). It was employed to investigate the graphene sample's morphology and to reveal the linear size of the graphene flakes obtained after the exfoliation of the graphite rods.

The structural parameters of the graphene sample were obtained by X-ray Powder Diffraction (XRD). The graphene pattern was recorded with a Bruker D8 Advance Diffractometer (Bruker, Austria, Vienna) using CuK_α radiation (1.5406 Å).

The presence of chemical functional groups on the graphene's surface was evidenced by X-Ray Photoelectron Spectroscopy (XPS). The data were collected at room temperature using a SPECS spectrometer equipped with a dual-anode Al/Mg X-ray source. The emitted photoelectrons, resulting from sample irradiation with an AlK X-ray source (1486.6 eV) operating at 200 W, were collected with a multi-channeltron detector and a PHOIBOS 150 2DCCD hemispherical energy analyzer. Data analysis and spectral curve fitting for the C 1s and O 1s regions were carried out using Casa XPS software (version 2.3.16, Casa Software Ltd., Wilmslow, Cheshire, UK). High-resolution peak fitting was performed employing a Gaussian–Lorentzian profile for each component, with nonlinear Shirley background model correction applied to account for instrumental and surface effects.

The electrochemical characteristics of the electrodes were studied with a Potentiostat/Galvanostat Instrument (PGSTAT-302N, Metrohm-Autolab B.V., KM Utrecht, The Netherlands) coupled with a three-electrode cell. As a counter electrode, a large Pt foil was employed, and the reference was an Ag|AgCl electrode (3 M KCl solution). Different electrochemical techniques were employed, such as the following: Linear Sweep Voltammetry (LSV), cyclic voltammetry (CV) and Electrochemical Impedance Spectroscopy (EIS).

## 3. Results and Discussions

The morphological and structural characterization of the graphene sample was performed using advanced techniques such as SEM, XRD and XPS. Such investigations were needed in order to correlate the synthesis procedure with the desired electro-catalytic properties of graphene. The morphology of the graphene sample found by SEM can be observed in Figure 1. Due to the mild exfoliation conditions, large sheets with linear sizes in the range of tens to hundreds of micrometers were produced. The wavy appearance of the sheets is evidenced in Figure 1b, this having a significant impact on the active area of the graphene-modified electrode. One of the effects is the increase in this area and, consequently, of the faradic current generated by catechol oxidation. Besides the large flakes,

smaller-sized flakes are also present, similar to 3D structures formed by the stacking of the monolayer sheets. Such structures are formed due to a small number of oxygen-containing groups attached to the graphene's surface. This observation is supported by the XRD study (see the next paragraph) which evidenced that the sample preponderantly contained few- and multi-layer graphene, and a small amount of graphene oxide (5%).
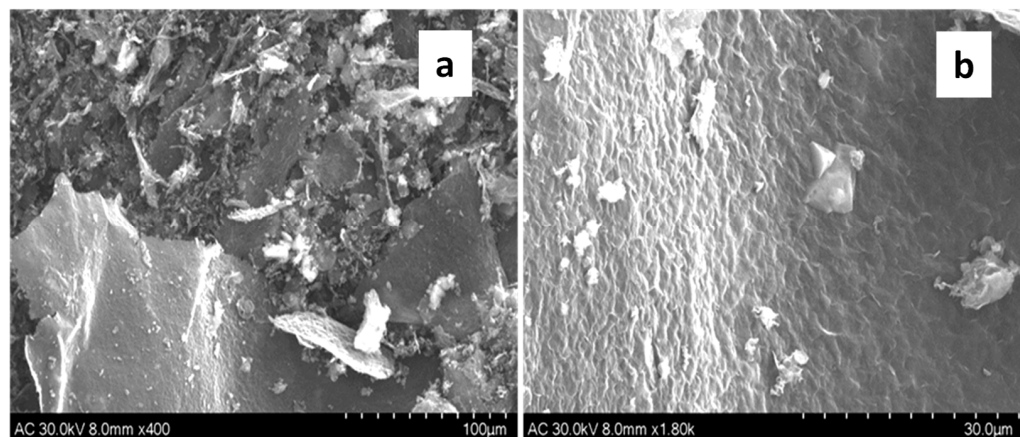
Figure 1. SEM micrographs of graphene sample, showing large sheets formed after electrochemical exfoliation of graphite bars; scale bar: 100 μm (**a**); 30 μm (**b**).

Next, X-ray Powder Diffraction and X-ray Photoelectron Spectroscopy were used for the structural characterization of the graphene. The XRD pattern (background subtracted) can be seen in Figure 2 and evidences three main peaks. The first two peaks are broad and of small intensities and appear at 2θ = 10 and 21.4 degrees, being attributed to graphene oxide (GO) and few-layer graphene (FLG), respectively [22]. The third peak at 2θ = 26.3 degrees is sharp and of high intensity, suggesting that it is composed of multi-layer graphene (MLG) [23]. After the de-convolution of the recorded pattern, the following structural parameters of the graphene sample were calculated: the number of layers (n) within the graphene flakes; the distance (d) between two adjacent layers; and the crystallite size (D) [24,25]. In addition, the FLG, MLG and GO amounts (%) in the sample were calculated and the results are listed in Table 1.
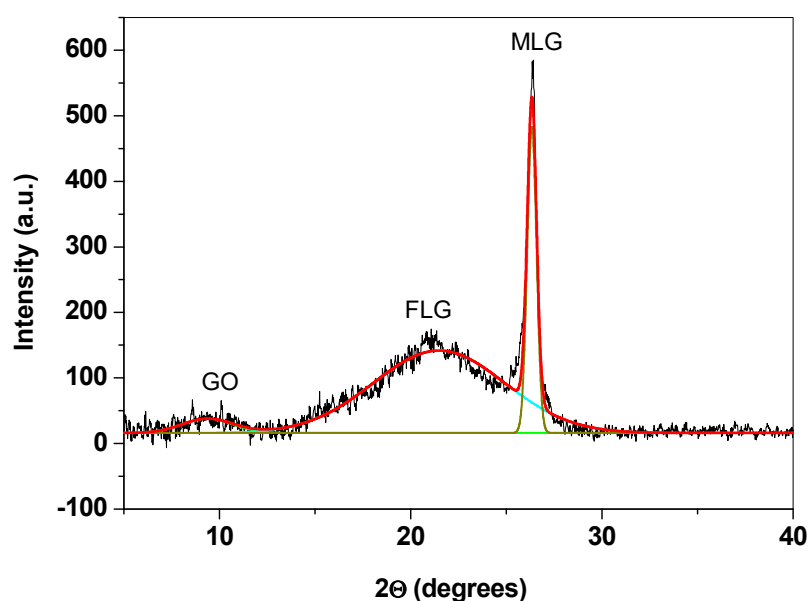

Figure 2. The XRD pattern of the graphene sample, evidencing the peaks attributed to GO, FLG and MLG.

Table 1. The structural parameters of the graphene sample calculated after the deconvolution of the XRD pattern: D—the crystallite size; d—the distance between two adjacent layers; n—the number of layers within the graphene flakes.

EGr Sample	D (nm)	d (nm)	n	Amount (%)
GO	3.2	0.944	2	5
FLG	1.24	0.414	3	20
MLG	19.4	0.339	57	75

The predominant number of flakes is that of MLG (75%), followed by FLG (20%) and GO (5%). In the case of FLG and MLG flakes, the corresponding interlayer distance is larger than that of pure graphite (0.334 nm), and this can be related to the presence of network defects in the flakes. Based on the previous work of Kampouris et al. [26], who showed that the edge plane of graphene is the origin of the high electron transfer rate, one can say that the MLG present in the sample has an important contribution to the observed electro-catalytic effect of the graphene-modified electrode.

XPS was employed to characterize the surface chemistry of the graphene, with a particular focus on the high-resolution C 1s and O 1s spectra. For the C 1s spectrum (Figure 3a), the deconvolution revealed multiple peaks corresponding to different bonding states of carbon, such as the following: sp^2 carbon in the graphene lattice (graphene backbone) at 284.49 eV, sp^3 carbon (defects or functional groups) at 285.6 eV and additional peaks corresponding to oxygenated groups such as hydroxyl (C–OH) at 286.43 eV, carbonyl (C=O) at 287.51 eV or epoxide (C–O–C) at 288.93 eV. The peak positions are consistent with the previous literature records of Estrade-Szwarckopf [27], Kovtun et al. [28] and Batzill [29]. A slight contribution to the spectrum's high binding energy (290.16 eV) was attributed to the graphitic carbons' $\pi \rightarrow \pi^*$ shake-up satellite band [30]. On the other hand, the deconvolution of the O 1s spectrum was analyzed in order to identify oxygen-containing functionalities, which are often present on the graphene's surface, providing critical information on the degree of oxidation and the presence of defects on the graphene's surface (Figure 3b). Three major components were necessary for the deconvolution of experimental data, in the form of C-O (531.45 eV), O-C=O/COOH (533.35 eV) and chemisorbed water (536.57 eV) contributions [31]. The C/O ratio was determined to be 0.16. This significantly influences graphene's electrochemical sensing capacity by altering its surface chemistry and increasing its reactivity, providing more active sites for electron transfer which can lead to an enhanced current response during catechol oxidation.
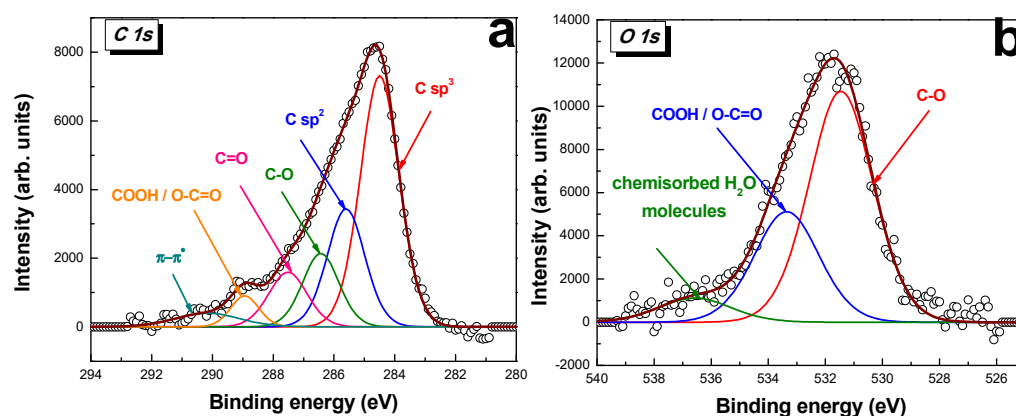
Figure 3. Deconvolution of high resolution C 1s (**a**) and O 1s (**b**) XPS states of graphene sample.

Next, electrochemical measurements were used for the investigation of the optimum experimental conditions necessary for catechol detection. Hence, the influence of the

solution pH on the catechol oxidation signal was investigated by CV in 10^{-4} M catechol. Figure 4a presents the CVs recorded within a 3.6–7.0 pH range, with a scan rate of 10 mV/s. Here, one can observe a significant variation in both anodic and cathodic peak intensity as well as of the corresponding peak potential with the solution pH. The anodic peak potential varies from +0.43 to +0.21 V and the linear equation which describes its variation with the pH is as follows: $E_{pa} = 0.63 - 0.06 \times pH$ (R = 0.990), having a slope close to 59 mV/pH. This indicates that the numbers of electrons and protons transferred during the oxidation of catechol are equal [32]. The anodic peak intensity (I_{pa}) also varies with the solution pH and reaches its maximum at pH 4.4; therefore, this value was selected as the optimum value for further investigations on catechol (Figure 4b,c).
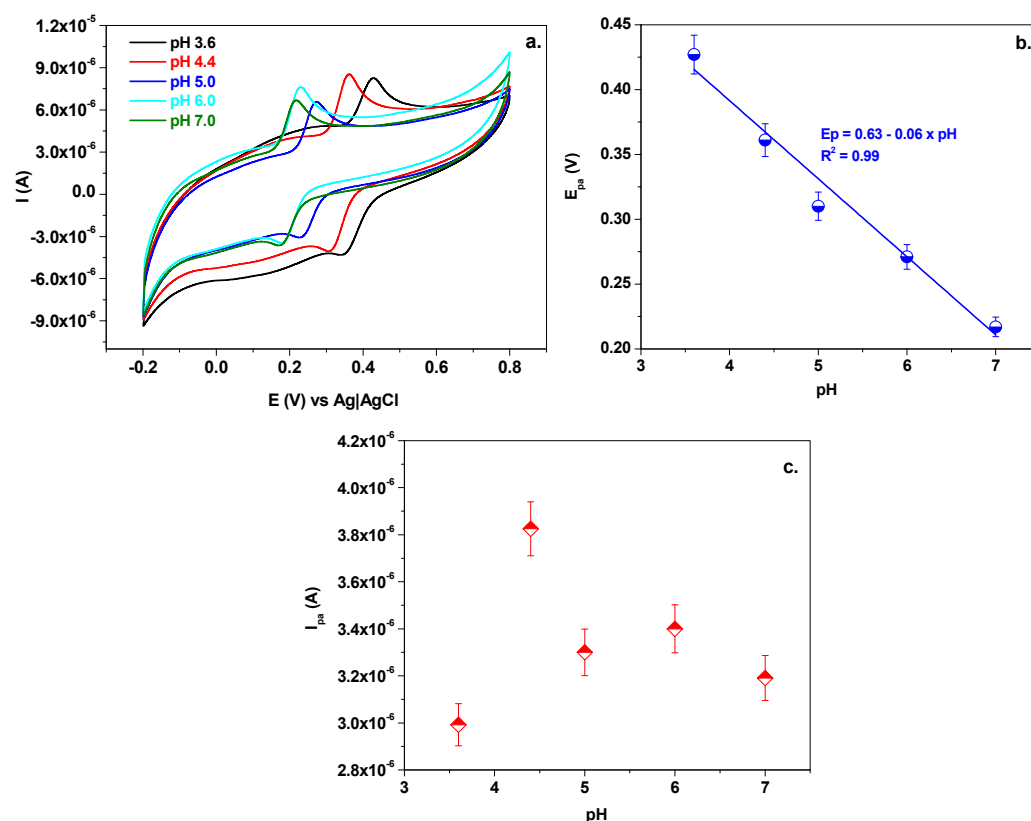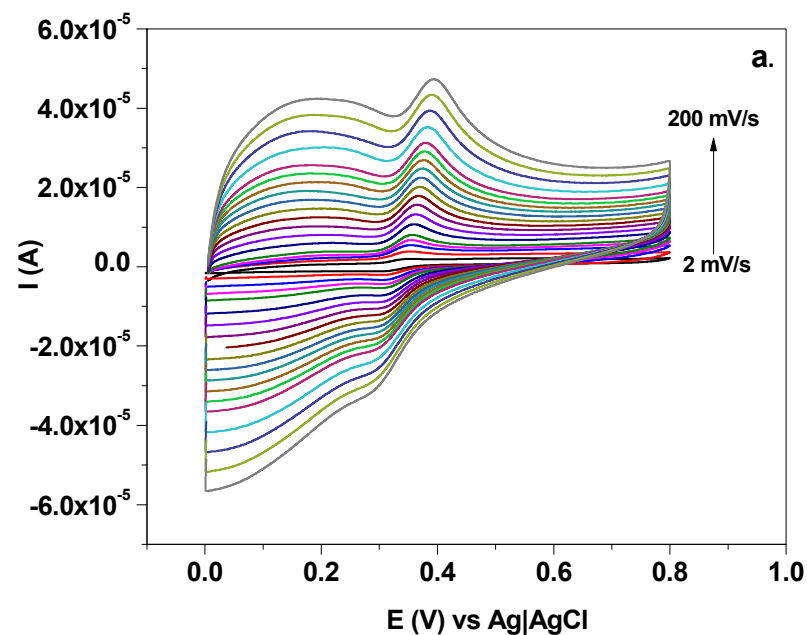

Figure 4. CVs recorded with EGr/GC electrode in solutions of different pH values, each containing 1×10^{-4} M catechol. 10 mV/s scan rate (**a**); variation in anodic peak potential (E_{pa}) with solution pH (**b**); variation in anodic peak current (I_{pa}) with solution pH (**c**).

The EGr/GC electrode was also employed for studying the influence of graphene on the electrochemical signal of catechol (Figure 5). With this electrode, a pair of well-defined oxidation/reduction signals were obtained at low potentials (+0.35 and +0.3 V, respectively) indicating that catechol undergoes a quasi-reversible redox process. For the bare GC, the oxidation and reduction signals are very broad and appear at different potentials (+0.63 and +0.08 V, respectively), demonstrating a sluggish transfer of electrons between the flat carbon surface and catechol. The peak intensities obtained with EGr/GC electrode are considerably higher (one order of magnitude) than that obtained from bare GC, demonstrating a favorable interaction between catechol molecules and the graphene surface, as well as an easy transfer of electrons.
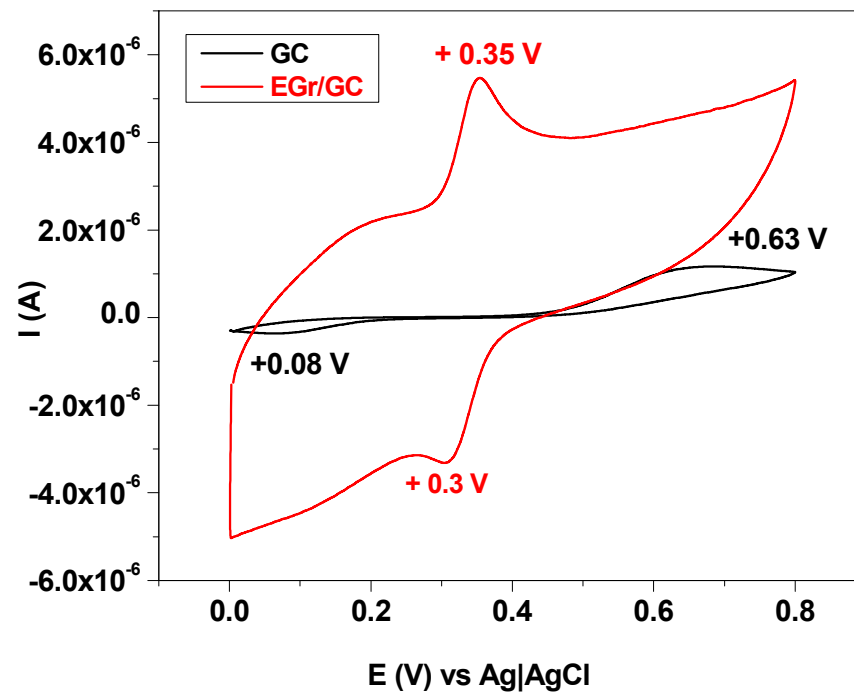
Figure 5. CVs recorded with EGr/GC (red) and GC (black) electrodes in solution containing 1×10^{-4} M catechol (pH 4.4 acetate); 10 mV/s scan rate.

In addition to this, it was worth investigating the influence of the scan rate on the catechol oxidation signal. In Figure 6a, the variations in the CV recordings with scan rate (2–200 mV/s) are represented. The corresponding anodic/cathodic peak currents were represented versus the square root of the scan rate ($\upsilon^{1/2}$), in which case linear plots were obtained. This indicates that the electron transfer reaction between catechol and the graphene surface is diffusion-controlled, rather than surface-controlled (Figure 6b). The corresponding linear regression equations are as follows: $I_{pa} = -4.44 \times 10^{-7} + 2.96 \times 10^{-5} \times \upsilon^{1/2}$ ($R^2 = 0.999$) and $I_{pc} = -8.74 \times 10^{-7} - 9.44 \times 10^{-6} \times \upsilon^{1/2}$ ($R^2 = 0.974$).


Figure 6. *Cont.*
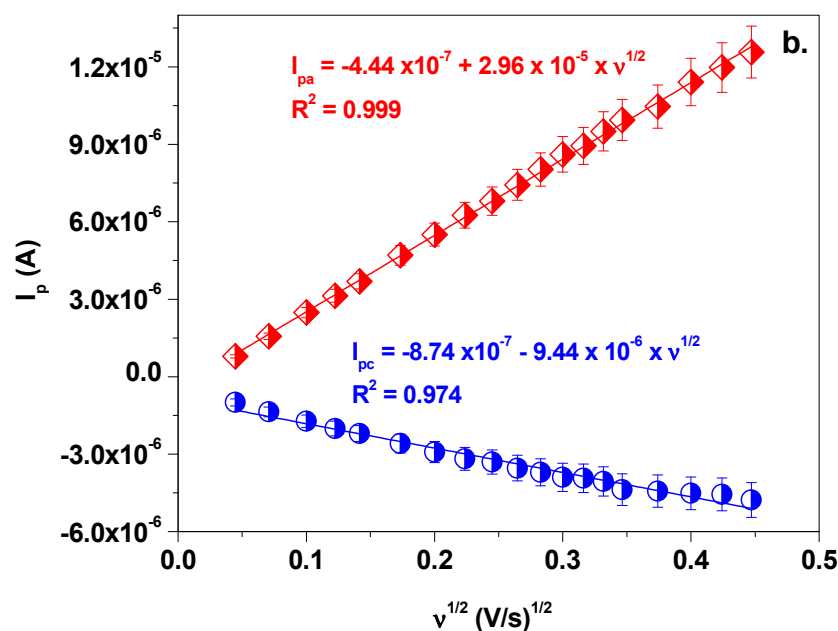
Figure 6. CVs recorded with EGr/GC electrode in solution containing 1×10^{-4} M catechol (pH 4.4 acetate) at various scan rates from 2 to 200 mV/s (**a**); linear representation of peak currents versus square root of scan rate (**b**).

Given an equal number of electrons and protons engaged in the reaction process, as proved by the information obtained from the effect of pH, a possible mechanism based on the transfer of two protons and two electrons was proposed according to Scheme 1, consistent with the previous reports of Xu et al. [33], Chen et al. [34], Indrajith Naik et al. [35] and Zheng and his collaborators [36].
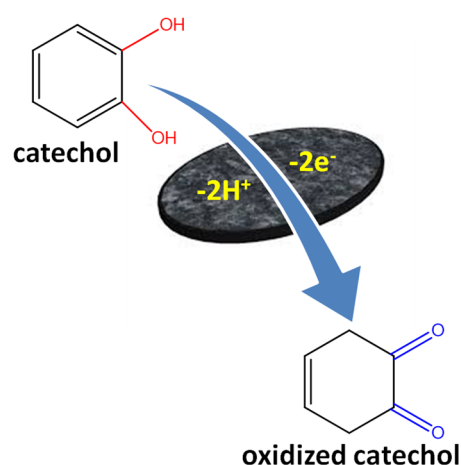
Scheme 1. The electrochemical reaction mechanism of catechol at the surface of the EGr/GC electrode.

The determination of the active area of the modified electrode was carried out with cyclic voltammetry experiments at different scanning rates, in the range of 2–100 mV/s, in the presence of 1×10^{-3} M redox indicator $K_4[Fe(CN)_6]$ and 0.2 M of KCl supporting electrolyte, using the Randles–Ševcik equation [37]:

$$I_{peak} = \pm 2.687 \times 10^5 AD^{1/2} \, n^{3/2} \, C \, v^{1/2}$$

where I_{peak} is the intensity of the anodic peak; A is the active area (cm²); D is the diffusion coefficient of $K_4[Fe(CN)_6]$; n is the number of electrons transferred in the redox process; v is the scan rate (V/s); and C is the concentration of $[K_4Fe(CN)_6]$ in the solution (mol/cm³).

The active areas of the bare and modified electrodes were determined from the slopes of I_{peak} versus $v^{1/2}$ plots (as visible in Figure S1 from the Electronic Supplementary Materials). As expected, the modified electrode has a considerably larger active area (0.047 cm^2) in comparison with that of bare GC (0.028 cm^2).

In order to further characterize the bare and the graphene-modified electrode, we employed the EIS technique. After recording the EIS spectrum of each electrode in 1×10^{-4} M catechol (pH 4.4 acetate; 0.1 to 1×10^5 Hz), we compared the spectra represented as Nyquist plots (Figure 7a,b). The inset of each figure represents the equivalent electrical circuit employed to fit the experimental data. The circuit for the bare GC electrode contains two resistances (the solution resistance, R_s, and the charge-transfer resistance, R_{ct}), the Warburg impedance (W) and a constant phase element (CPE) that simulates non-ideal behavior of the capacitor [38]. It is important to point out that the semicircle in the measured Nyquist plot has a flattened shape, rather than an ideal semicircle shape. This can be attributed to some inhomogeneity present at the electrode's surface (e.g., the density of current, the adsorption of analytes with the coverage of the electrode surface) [39] The CPE is often used to describe this phenomenon [40]. The large semicircle in the high–medium frequency range is due to the large charge-transfer resistance (R_{ct} = 82.7 kΩ) of the bare electrode towards catechol oxidation. The straight line from the medium to low frequencies is characteristic of the diffusion of catechol molecules within the electric double-layer, and is described by the Warburg impedance.

As concerned the EGr/GC electrode, the equivalent electrical circuit (Figure 7b) employed to fit the experimental data contains the following elements: the solution resistance; the charge-transfer resistance, which in this case has a considerably lower value (R_{ct} = 313 Ω) indicating a swift transfer of electrons between graphene and catechol molecules; and two constant phase elements (CPE_1 and CPE_2) due to the high porosity of the graphene layer. The EIS results revealed that the addition of graphene on top of the GC electrode had a significant impact on the R_{ct} value, considerably decreasing its value. The steep rising trend of the imaginary part (Z'') with respect to the real part (Z') of the impedance (at low frequencies) can be attributed to the capacitive behavior of the graphene-modified electrode.

Based on the determined R_{ct} values, the apparent heterogeneous electron transfer rate (k_{app}) was calculated for each electrode, using the following equation [37]:

$$k_{app} = \frac{RT}{n^2 F^2 A R_{ct} C} \tag{1}$$

where n is the number of electrons transferred during the redox reaction (n = 2); F is the Faraday constant (96,485 C/mol); R is the ideal gas constant (8.314 J/(mol·K)); T is the temperature (298 K); A is the active area of the electrode (0.0472 cm^2 for EGr/GC and 0.028 cm^2 for GC); R_{ct} is the charge-transfer resistance obtained from the fitted Nyquist plots (Ω); and C is the concentration of the catechol solution (10^{-7} mol/cm^3).

After calculations, it was found that the k_{app} value of EGr/GC was 4.5×10^{-2} cm/s, being two orders of magnitude higher than that corresponding to bare GC (2.87×10^{-4} cm/s). Hence, the presence of graphene on top of the GC electrode not only increased the active area of the electrode but also highly promoted the transfer of electrons from catechol molecules to the GC substrate.

The LSV was next employed to determine some important analytical parameters, such as the following: the electrode sensitivity, the linear range in catechol solutions, the limit of quantification (LOQ) and the limit of detection (LOD). Figure 8 presents the LSV signals recorded with the graphene-modified GC (a) and bare GC (b) within different concentration ranges, with a scan rate of 10 mV/s. Marked differences between the two electrodes can

be observed not only in the recorded LSVs but also in the linear plots of the anodic peak current, I_{pa}, versus catechol concentration (Figure 9). Hence, in the case of the EGr/GC electrode, the recorded LSVs revealed no shift in the anodic peak potential with the catechol concentration. This is in full agreement with the previous findings that the oxidation process of catechol is a diffusion-controlled one, and not an adsorption-controlled one [41,42]. In the case of the GC electrode, the shift in the anodic peak potential with catechol concentration is large (50 mV), indicating the probability of adsorption of the oxidized molecules on the flat GC surface.
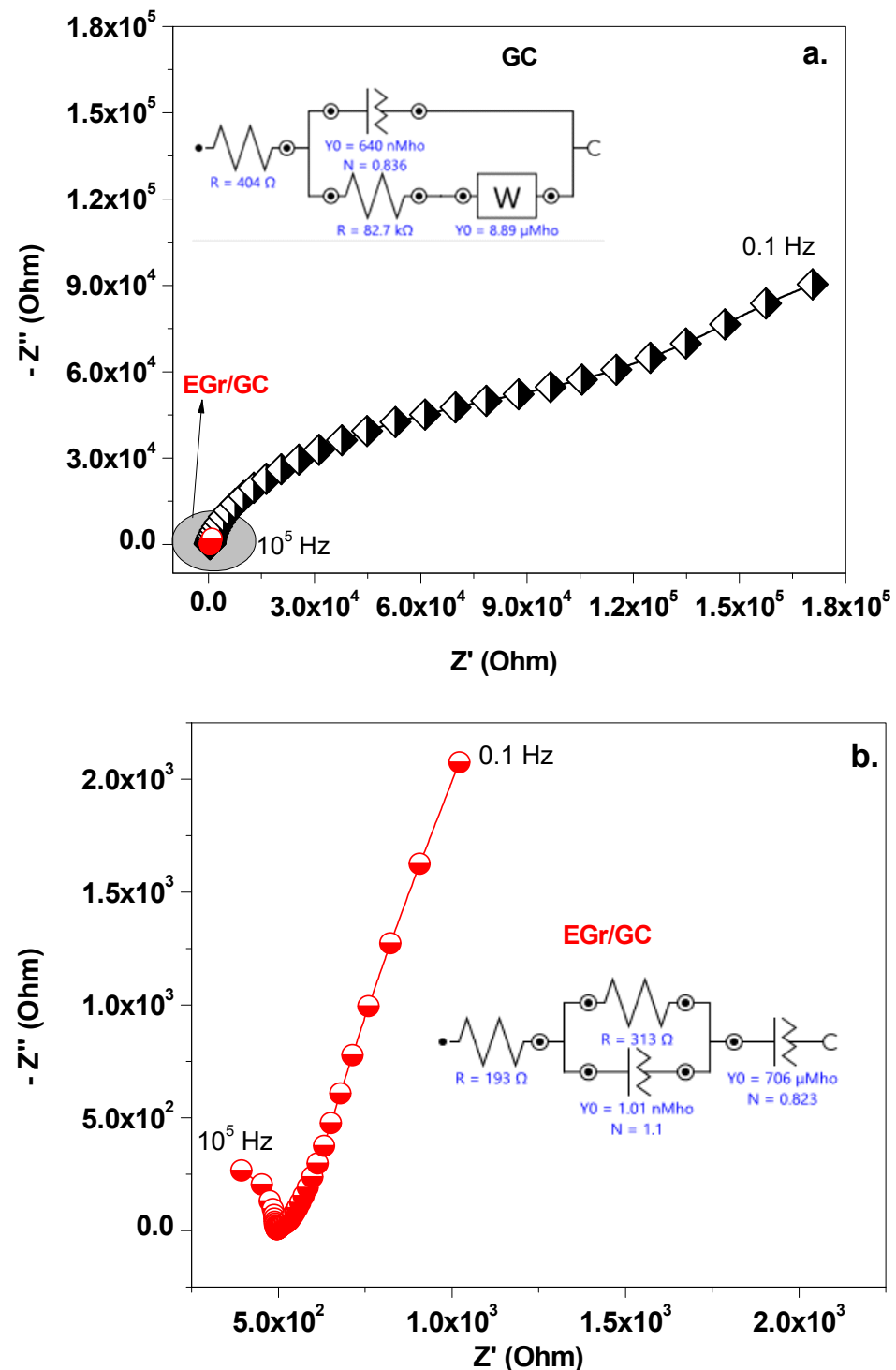

Figure 7. Nyquist plots obtained in 1×10^{-4} M catechol (acetate pH 4.4) with bare GC (**a**) and EGr/GC electrode (**b**); insets: equivalent electrical circuit employed for each electrode.
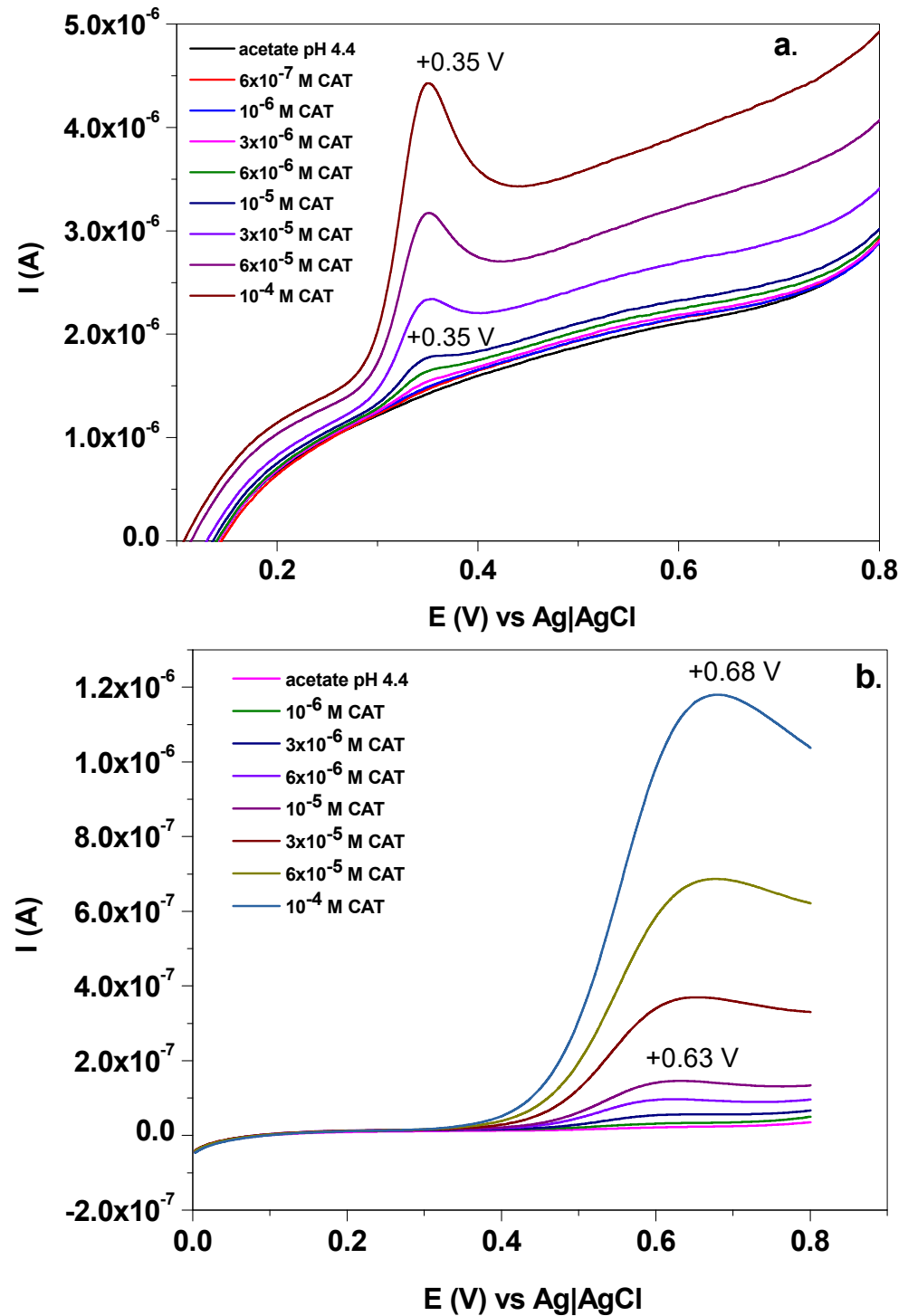
Figure 8. LSVs recorded in solutions containing catechol of various concentrations, from 6×10^{-7} to 1×10^{-4} M (EGr/GC electrode), 10 mV/s scan rate (**a**); LSVs recorded in solutions containing catechol of various concentrations, from 1×10^{-6} to 1×10^{-4} M (GC electrode), 10 mV/s scan rate (**b**).

Next, the analytical parameters for the two electrodes were determined from the corresponding calibration plots, by representing I_{pa} versus catechol concentration. The plots can be seen in Figure 9, along with the linear regression equations that fit the plots. For the EGr/GC electrode, the linear range for catechol was wide, from 6×10^{-7} to 1×10^{-4} M catechol; the LOQ was 6×10^{-7} M; and the LOD was 1.82×10^{-7} M (LOD = LOQ/3.3). In addition, the sensitivity was five times higher than that corresponding to bare GC, proving the excellent electro-catalytic properties of the graphene-modified electrode. An excellent

reproducibility of the peak signal was obtained, as revealed by the successive measurements recorded with the EGr/GC electrode. Between the measurements, the graphene-modified electrode was immersed in water for 30 min and then cycled in pH 4.4 acetate buffers until no peak was revealed (from 0.0 to +0.8 V vs. Ag|AgCl potential range; 50 mV/s).
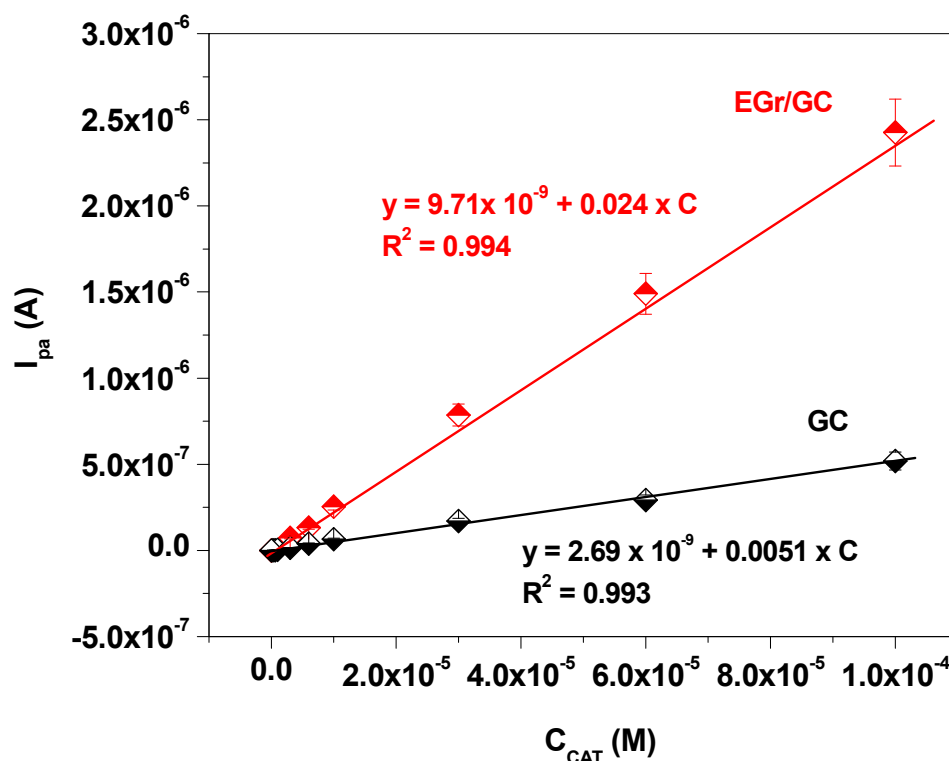
Figure 9. Calibration plots for catechol obtained with EGr/GC (red) and GC (black) electrodes.

Previous modified electrodes found in the literature were compared with the developed graphene-based sensing platform, confirming its good analytical performances and suggesting its practical applicability in catechol assays (please see Table 2).

Table 2. A comparison of the analytical performance of EGr/GC with other electrochemical sensors for the determination of catechol.

Electrode	Linear Range (μM)	LOD (μM)	Technique	Reference
$Fe_3O_4–TiO_2$/GCE $Fe_3O_4–TiO_2–Fe_3O_4$ nanoparticles as dopant on mesoporous TiO_2 GCE—glassy carbon electrode	100–500	45	CV	[43]
CMK-3-Nafion/GCE CMK-3-Nafion—mesoporous carbon CMK-3/nafioncomposite GCE—glassy carbon electrode	0.5–35	0.1	CV	[44]
[Cu(Sal-β-Ala)(3,5-DMPz)2]/SWCNTs/GCE copper(II) complex [Cu(Sal-β-Ala) (3,5-DMPz)$_2$] (Sal = salicylaldehyde, β-Ala = β-alanine, 3,5-DMPz = 3,5-dimethylpyrazole) and single-walled carbon nanotubes (SWCNTs)	5–69.5	3.5	DPV	[45]

Table 2. *Cont.*

| Electrode	Linear Range (μM)	LOD (μM)	Technique	Reference
PNA(ii)/Cd(0.02)-ZnWO$_4$/CPE PNA(ii)/Cd(0.02)-ZnWO$_4$—poly-(nicotinic acid) film and Cd-doped ZnWO$_4$ (Cd-ZnWO$_4$) nanoneedles organic–inorganic nanocomposite CPE–carbon paste electrode	2–35	0.17	DPV	[14]
PASA/MWNTs/GCE PASA/MWNTs—poly-amidosulfonic acid and multi-wall carbon nanotubes composite GCE—glassy carbon electrode	6–700	1	DPV	[46]
PNR/MCPE PNR—poly (neutral red) MCPE—modified carbon paste electrode	0.1–100	6.46	DPV	[47]
(CMWNTs-NHCH2CH2NH)6/GCE (CMWNTs-NHCH2CH2NH)6—carboxylated multi-wall carbon nanotubes layer-by-layer self-assembled film	5–80	1	DPV	[48]
LDHf/GCE LDHf—Zn/Al-layered double hydroxide film GCE—glassy carbon electrode	3–1500	1.2	DPV	[49]
RGO–MWNTs/GCE RGO–MWNTs—reduced graphene oxide and multi-wall carbon nanotube hybrid materials GCE—glassy carbon electrode	5.5–540	1.8	DPV	[50]
GNPs/CNF/Au GNPs/CNF—carbon nanofibers and gold nanoparticles nanocomposite	5–350	0.36	DPV	[51]
BG/GCE BG—Boron-doped graphene GCE—glassy carbon electrode	1–75	0.2	DPV	[52]
Pt–MnO$_2$/GCE Pt–MnO$_2$—Pt–MnO$_2$ composite film	15–447	4.54	DPV	[53]
p-Glu/GCE p-Glu—electropolymerized film of glutamic acid GCE—glassy carbon electrode	5–80	0.8	DPV	[54]
poly-p-ABA/GCE poly-p-ABA—poly(p-aminobenzoic acid) GCE—glassy carbon electrode	2.0–900	0.5	DPV	[55]
AuNPs/Fe$_3$O$_4$-APTES-GO/GCE AuNPs/Fe$_3$O$_4$-APTES-GO—Fe$_3$O$_4$-functionalized graphene oxide–gold nanoparticle composite GCE—glassy carbon electrode	2–145	0.8	AMP	[56]
GCE@Cu-PPy Cu-PPy—copper–polypyrrole composite GCE—glassy carbon electrode	0.02–2500	0.152	AMP	[57]
OMC/GC OMC—ordered mesoporous carbon GC—glassy carbon electrode	10–300	0.1	AMP	[58]

Table 2. *Cont.*

Electrode	Linear Range (µM)	LOD (µM)	Technique	Reference
GCE/polyPATT/Den(AuNP)/tyrosinase GCE—glassy carbon electrode polyPATT/Den(AuNP)/tyrosinase—gold nanoparticles-encapsulated dendrimer	0.005–120	0.002	AMP	[59]
EGr/GC	0.6–100	0.182	LSV	* current work

Next, we tested the influence of interfering species, hydroquinone (HQ) and resorcinol (REZ) on the performances of the EGr/GC electrode. The reason for choosing such compounds is related to the fact that they are catechol isomers, so they may have similar electrochemical properties. Hence, the signal of catechol was recorded by LSV in pH 4.4 acetate solutions containing increasing concentrations of hydroquinone (1×10^{-5} M; 5×10^{-5} M and 1×10^{-4} M), see Figure 10a. In this figure, the HQ signal is well defined and appears at a potential of +0.26 V, close to that of catechol molecules (+0.35 V). By increasing the HQ concentration, a change in the capacitive current may be observed in the recorded LSVs, with no influence on the catechol peak potential (+0.35 V). Additionally, the peak current of catechol is only slightly diminished by HQ when its concentration is low (1×10^{-5} M and 5×10^{-5} M; see the green and cyan curves in comparison with the red one). At a high HQ concentration (1×10^{-4} M), the capacitive current is considerably higher and the peak current of catechol is smaller, indicating a competitive interaction between the HQ and CAT molecules with the graphene surface.

Next, resorcinol was tested as an interfering molecule during catechol detection. Increasing concentrations of resorcinol (1×10^{-5} M, 5×10^{-5} M and 1×10^{-4} M) were added to solutions containing catechol, and the recorded LSV signals can be seen in Figure 10b. In contrast with catechol, the oxidation signal of resorcinol appears at higher potential (+0.75 V) due to the different reactivity of these isomers. Its presence in the solution has an influence on the capacitive current, decreasing it, and a lower influence on the oxidation peak of catechol, regardless of its concentration.

In addition, we tested the effect of other interfering species (potassium chloride, sodium nitrite, sodium bicarbonate and their mixture) to the response of EGr/GC in the presence of catechol. The results are shown in Figure S2, in the Electronic Supplementary Materials. Here, one can see that these interfering species, with the exception of KCl (Figure S2a), have a very small effect on the oxidation signal of catechol. It is interesting to mention that KCl also has a negligible effect when it is in a mixture with sodium nitrite and sodium bicarbonate (Figure S2d). The oxidation signal of nitrite can be observed at high potential (+0.8 V vs. Ag│AgCl), but without an effect on catechol oxidation (Figure S2c,d).

Before testing the practical applicability of the developed sensor, we tested the electrode stability by cyclic voltammetry (40 cycles) in a 4.4 pH acetate buffer solution containing 1×10^{-4} M catechol. Excellent stability was obtained in time, proving the usability of the graphene-modified electrode for repetitive measurements (Figure S3 from the Electronic Supplementary Materials).
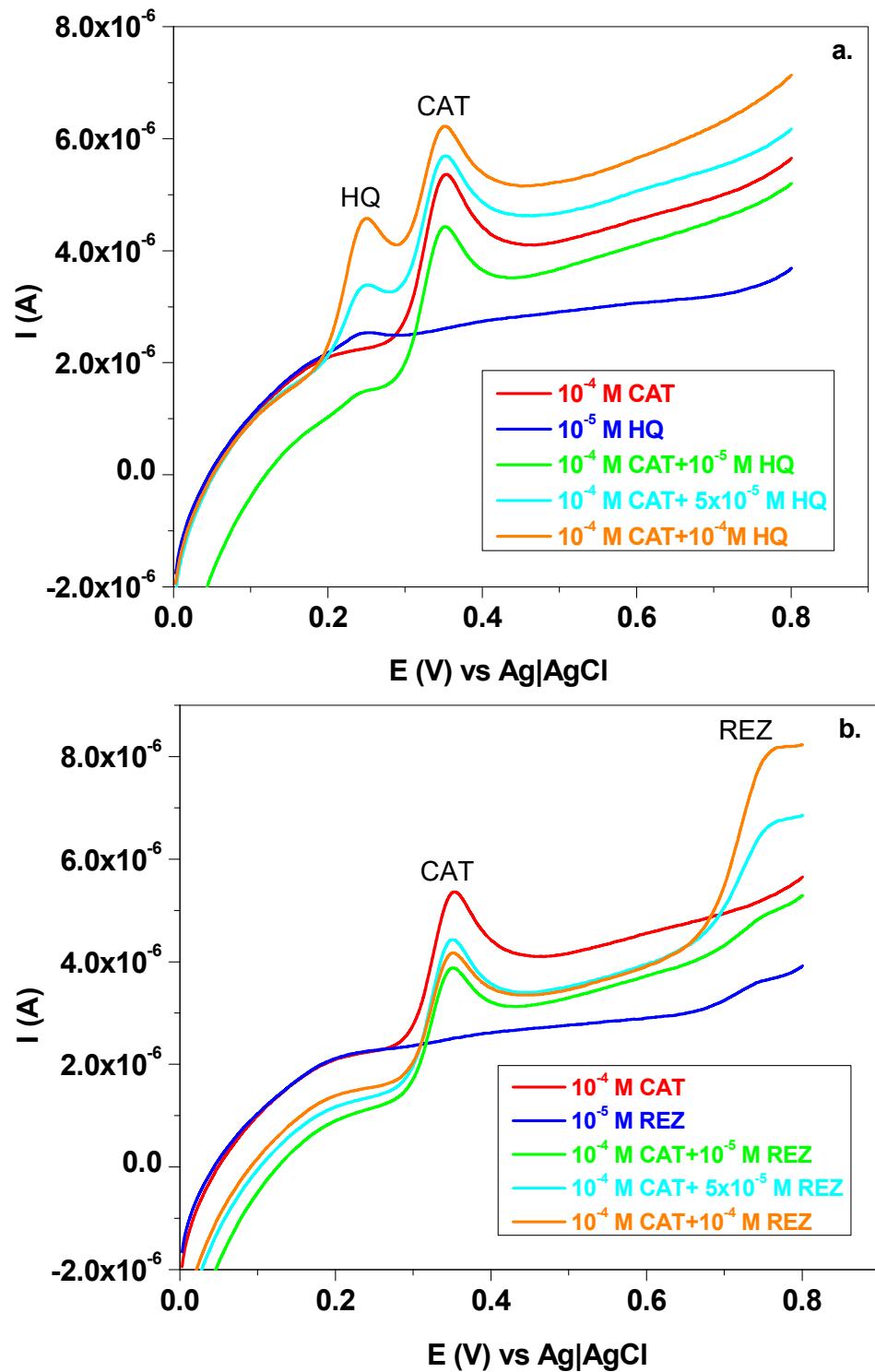
Figure 10. LSVs recorded with EGr/GC electrode in pH 4.4 acetate solutions containing 1×10^{-4} M catechol (red) and increasing concentrations of HQ: 1×10^{-5} M (green), 5×10^{-5} M (cyan) and 1×10^{-4} M (orange); 10 mV/s scan rate (**a**). LSVs recorded with EGr/GC electrode in pH 4.4 acetate solutions containing 1×10^{-4} M catechol (red) and increasing concentrations of REZ: 1×10^{-5} M (green), 5×10^{-5} M (cyan) and 1×10^{-4} M (orange); 10 mV/s scan rate (**b**).

The applicability of the graphene-modified electrode was tested in tap water. The pH of the tap water was brought to the value of pH 4.4 and 100 μL of 1×10^{-4} M catechol was put in a beaker containing the tap water (5 mL final volume). The obtained concentration was considered to be an "unknown" concentration ($C_x = 3 \times 10^{-6}$ M). LSV was recorded

in this solution and a small signal attributed to catechol was observed at a potential of $+0.35$ V (see Figure 11a, red curve). Next, increasing volumes (100, 150, 200 µL) of 1×10^{-4} M catechol were spiked into three beakers (which also contained C_x) and the corresponding LSV curves were recorded (black, blue and pink curves). The obtained concentrations ($C_1 = 2 \times 10^{-6}$ M; $C_2 = 3 \times 10^{-6}$ M; $C_3 = 4 \times 10^{-6}$ M) were denoted to the added concentrations, since the value of C_x was ignored in the three beakers. After plotting the anodic peak currents versus the added concentrations (C_{added}) of catechol, a straight line was obtained, allowing the determination of the "unknown" catechol content in the tap water ($C_{found} = 3.06 \times 10^{-6}$ M), giving a recovery of 102% (recovery = C_{found}/C_x), as seen in Figure 11b.
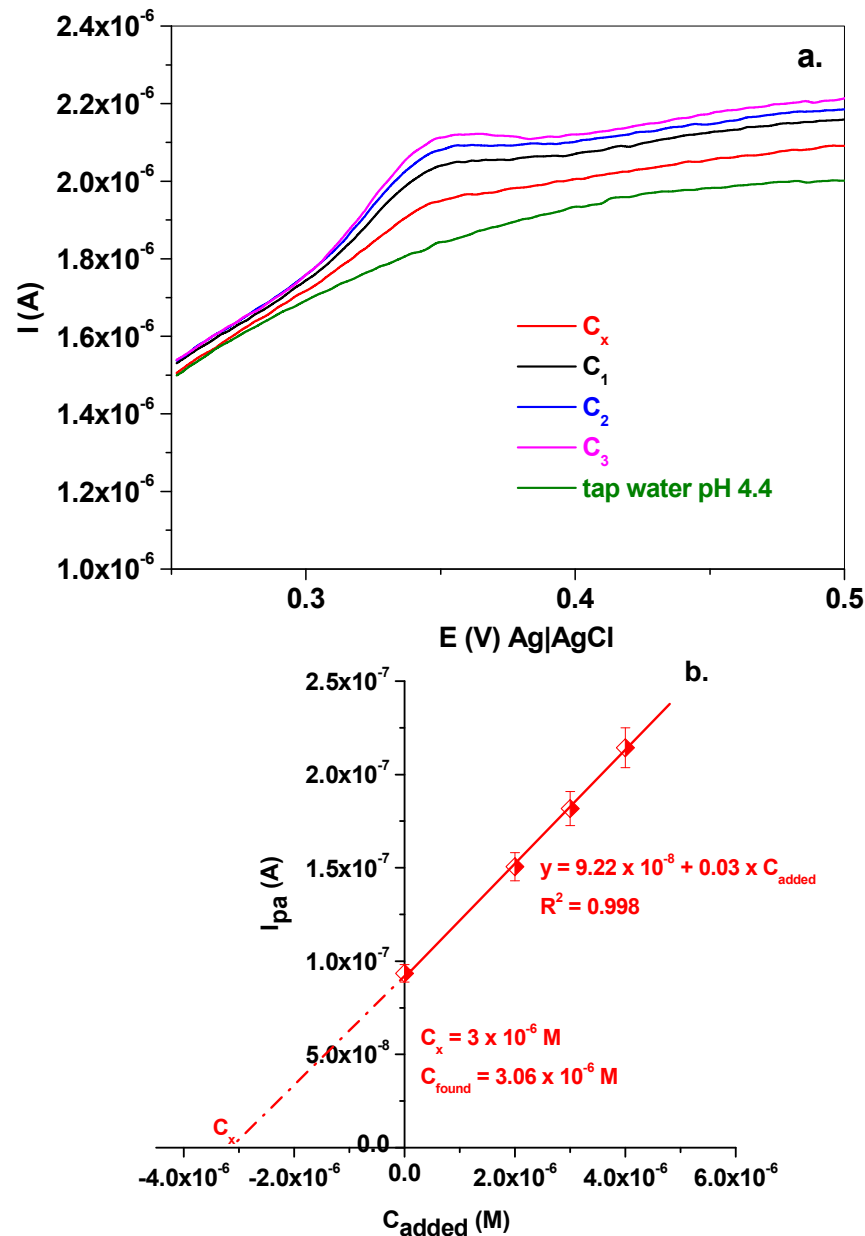
Figure 11. The LSVs recorded in tap water containing the "unknown" catechol solution (red curve) and the added catechol concentrations ($C_1 = 2 \times 10^{-6}$ M—black; $C_2 = 3 \times 10^{-6}$ M—blue; and $C_3 = 4 \times 10^{-6}$ M—pink curve); the green curve was recorded in tap water, without catechol; scan rate 10 mV/s (**a**). The corresponding standard addition plot obtained by representing the anodic peak current, I_{pa}, versus the added catechol concentrations, C_{added} (**b**).

4. Conclusions

The graphene sample synthesized by the electrochemical exfoliation of graphite rods was morphologically and structurally characterized by advanced techniques, such as SEM, XRD and XPS. The XRD pattern revealed that the sample contains flakes composed of few-layer and multi-layer graphene as well as a small amount of graphene oxide. The sample was drop-casted on top of a glassy carbon electrode and the electrochemical properties of the bare and graphene-modified electrodes were studied. The EIS technique revealed that the graphene-modified electrode has a low charge-transfer resistance (R_{ct} = 313 Ω) in comparison with that obtained for the bare glassy carbon (R_{ct} = 82.7 kΩ). Marked differences between the two electrodes were also observed in the linear plots of the anodic peak currents, I_{pa}, versus catechol concentration. For the graphene-modified electrode, the analytical parameters were better than those corresponding to bare GC, proving its applicability in catechol detection.

References

1. Piñeiro, Z.; Palma, M.; Barroso, C.G. Determination of catechins by means of extraction with pressurized liquids. *J. Chromatogr. A* **2004**, *1026*, 19–23. [CrossRef] [PubMed]
2. IARC Working Group on the Evaluation of Carcinogenic Risks to Humans. Re-Evaluation of Some Organic Chemicals, Hydrazine and Hydrogen Peroxide. Lyon (FR): International Agency for Research on Cancer, 1999. (IARC Monographs on the Evaluation of Carcinogenic Risks to Humans, No. 71.) Catechol. Available online: https://www.ncbi.nlm.nih.gov/books/NBK498783/ (accessed on 12 November 2024).
3. Hamamoto, T.; Umemura, S. Phenol derivatives; catechol. In *Ullmann's Encyclopedia of Industrial Chemistry*, 5th rev. ed.; Gerhartz, W., Yamamoto, Y.S., Eds.; VCH Publishers: New York, NY, USA, 1991; Volume A1, pp. 342–346.
4. Goldstein, D.S. *Primer on the Autonomic Nervous System*, 3rd ed.; Academic Press: Cambridge, MA, USA, 2012; pp. 37–43. [CrossRef]

5.   Bhat, R.V.; Subrahmanyam, V.V.; Sadler, A.; Ross, D. Bioactivation of catechol in rat and human bone marrow cells. *Toxicol. Appl. Pharmacol.* **1988**, *94*, 297–304. [CrossRef]

6.   Atchison, M.; Chu, C.; Kakunaga, T.; Van Duuren, B.L. Chemical cocarcinogenesis with the use of a subclone derived from Balb/3T3 cells with catechol as cocarcinogen. *J. Natl. Cancer Inst.* **1982**, *69*, 503–508.

7.   Li, Q.; Aubrey, M.T.; Christian, T.; Freed, B.M. Differential inhibition of DNA synthesis in human T cells by the cigarette tar components hydroquinone and catechol. *Fundam. Appl. Toxicol.* **1997**, *38*, 158–165. [CrossRef] [PubMed]

8.   Coros, M.; Pogacean, F.; Magerusan, L.; Rosu, M.-C.; Porav, A.-S.; Socaci, C.; Bende, A.; Stefan-van Staden, R.-I.; Pruneanu, S. Graphene-porphyrin composite synthesis through graphite exfoliation: The electrochemical sensing of catechol. *Sensors Actuators B Chem.* **2018**, *256*, 665–673. [CrossRef]

9.   Magerusan, L.; Pogacean, F.; Cozar, B.-I.; Tripon, S.-C.; Pruneanu, S. Harnessing Graphene-Modified Electrode Sensitivity for Enhanced Ciprofloxacin Detection. *Int. J. Mol. Sci.* **2024**, *25*, 3691. [CrossRef] [PubMed]

10. Chetankumar, K.; Swamy, B.E.K.; Sharma, S.C.; Hariprasad, S.A. An efficient electrochemical sensing of hazardous catechol and hydroquinone at direct green 6 decorated carbon paste electrode. *Sci. Rep.* **2021**, *11*, 15064. [CrossRef] [PubMed]

11. Chetankumar, K.; Swamy, B.E.K.; Sharma, S.C. Electrochemical preparation of poly (direct yellow 11) modified pencil graphite electrode sensor for catechol and hydroquinone in presence of resorcinol: A voltammetric study. *Microchem. J.* **2020**, *156*, 104979. [CrossRef]

12. Chetankumar, K.; Swamy, B.E.K.; Sharma, S.C. Poly (benzoguanamine) modified sensor for catechol in presence of hydroquinone: A voltammetric study. *J. Electroanal. Chem.* **2019**, *849*, 113365. [CrossRef]

13. Teradale, A.B.; Lamani, S.D.; Ganesh, P.S.; Swamy, B.E.K.; Das, S.N. Poly-nile blue based electrochemical sensor for catechol and hydroquinone. *Anal. Bioanal. Electrochem.* **2019**, *11*, 1176–1190.

14. Dang, Y.; Wang, X.; Cui, R.; Chen, S.; Zhou, Y. A novel electrochemical sensor for the selective determination of hydroquinone and catechol using synergic effect of electropolymerized nicotinic acid film and Cd-doped $ZnWO_4$ nanoneedle. *J. Electroanal. Chem.* **2019**, *834*, 196–205. [CrossRef]

15. Zhao, L.; Yu, J.; Yue, S.; Zhang, L.; Wang, Z.; Guo, P.; Liu, Q. Nickel oxide/carbon nanotube nanocomposites prepared by atomic layer deposition for electrochemical sensing of hydroquinone and catechol. *J. Electroanal. Chem.* **2018**, *808*, 245–251. [CrossRef]

16. Wang, Y.; Xiong, Y.Y.; Qu, J.Y.; Qu, J.H.; Li, S.F. Selective sensing of hydroquinone and catechol based on multiwalled carbon nanotubes/polydopamine/gold nanoparticles composites. *Sensors Actuators B Chem.* **2016**, *223*, 501–508. [CrossRef]

17. Wang, J.; Yang, J.; Xu, P.; Liu, H.; Zhang, L.; Zhang, S.; Tian, L. Gold nanoparticles decorated biochar modified electrode for the high performance simultaneous determination of hydroquinone and catechol. *Sens. Actuators B Chem.* **2020**, *306*, 127590. [CrossRef]

18. Bahadır, E.B.; Sezgintürk, M.K. Applications of graphene in electrochemical sensing and biosensing. *TrAC Trends Anal. Chem.* **2016**, *76*, 1–14. [CrossRef]

19. da Silva, A.D.; Paschoalino, W.J.; Damasceno, J.P.V.; Kubota, L.T. Structure, Properties, and Electrochemical Sensing Applications of Graphene-Based Materials. *ChemElectroChem* **2020**, *7*, 4508–4525. [CrossRef]

20. Fu, L.; Zheng, Y.; Li, X.; Liu, X.; Lin, C.-T.; Karimi-Maleh, H. Strategies and Applications of Graphene and Its Derivatives-Based Electrochemical Sensors in Cancer Diagnosis. *Molecules* **2023**, *28*, 6719. [CrossRef]

21. Manjunatha, J.G. *Graphene-Based Sensors*; IOP Publishing Ltd.: Bristol, UK, 2023; ISBN 978-0-7503-5578-0/978-0-7503-5576-6. [CrossRef]

22. Storm, M.M.; Johnsen, R.E.; Norby, P. In situ X-ray powder diffraction studies of the synthesis of graphene oxide and formation of reduced graphene oxide. *J. Solid State Chem.* **2016**, *240*, 49–54. [CrossRef]

23. Magerusan, L.; Pogacean, F.; Leostean, C.; Pruneanu, S. Selective graphene-based electrochemical sensing platform for enhanced sulfamethoxazole assay. *Microchem. J.* **2024**, *197*, 109886. [CrossRef]

24. Warren, B.E. *X-Ray Diffraction*; Addison-Wesley: Reading, MA, USA; Dover: Mineola, NY, USA, 1969; ISBN 0-486-66317-5, 1969/1990.

25. Pope, C.G. X-Ray Diffraction and the Bragg Equation. *Chem. Educ.* **1997**, *74*, 129. [CrossRef]

26. Kampouris, D.K.; Banks, C.E. Exploring the physicoelectrochemical properties of graphene. *Chem. Commun.* **2010**, *46*, 8986–8988. [CrossRef] [PubMed]

27. Estrade-Szwarckopf, H. XPS photoemission in carbonaceous materials: A "defect" peak beside the graphitic asymmetric peak. *Carbon* **2004**, *42*, 1713–1721. [CrossRef]

28. Kovtun, A.; Jones, D.; Dell'Elce, S.; Treossi, E.; Liscio, A.; Palermo, V. Accurate chemical analysis of graphene-based materials using X-ray photoelectron spectroscopy. *Carbon* **2019**, *143*, 268–275. [CrossRef]

29. Batzill, M. The surface science of graphene: Metal interfaces, CVD synthesis, nanoribbons, chemical modifications, and defects. *Surf. Sci. Rep.* **2012**, *67*, 83–115. [CrossRef]

30. Magerusan, L.; Pogacean, F.; Pruneanu, S. Eco-friendly synthesis of sulphur-doped graphenes with applicability in caffeic acid electrochemical assay. *Bioelectrochemistry* **2022**, *148*, 108228. [CrossRef] [PubMed]

31. Xie, W.; Chan, C.M. *Surface Analysis of Graphene and Graphite. Applications and Use of Diamond*; David, G., Ed.; IntechOpen: London, UK, 2023. [CrossRef]

32. Li, J.; Qu, J.; Yang, R.; Qu, L.; Harrington, P.d.B. A sensitive and selective electrochemical sensor based on graphene quantum dot/gold nanoparticle nanocomposite modified electrode for the determination of quercetin in biological samples. *Electroanalysis* **2016**, *28*, 1322–1330. [CrossRef]

33. Xu, Y.; Yu, Y.; Xue, S.; Ma, X.; Tao, H. Innovative electrochemical sensor based on graphene oxide aerogel wrapped copper centered metal-organic framework to detect catechol. *J. Electroanal. Chem.* **2021**, *899*, 115686. [CrossRef]

34. Chen, T.; Liu, C.; Liu, X.; Zhu, C.; Zheng, D. Simultaneous Electrochemical Detection of Catechol and Hydroquinone Based on a Carbon Nanotube Paste Electrode Modified with Electro-Reduced Graphene Oxide. *Int. J. Mol. Sci.* **2024**, *25*, 9829. [CrossRef] [PubMed]

35. Indrajith Naik, E.; Sunil Kumar Naik, T.S.; Pradeepa, E.; Singh, S.; Naik, H.S.B. Design and fabrication of an innovative electrochemical sensor based on Mg-doped ZnO nanoparticles for the detection of toxic catechol. *Mater. Chem. Phys.* **2022**, *281*, 125860. [CrossRef]

36. Zheng, S.; Zhang, N.; Li, L.; Liu, T.; Zhang, Y.; Tang, J.; Guo, J.; Su, S. Synthesis of Graphene Oxide-Coupled CoNi Bimetallic MOF Nanocomposites for the Simultaneous Analysis of Catechol and Hydroquinone. *Sensors* **2023**, *23*, 6957. [CrossRef]

37. Zanello, P. *Inorganic Electrochemistry: Theory, Practice and Application*; The Royal Society of Chemistry: London, UK, 2003; ISBN 0-85404-661-5.

38. Ahmed, J.; Rakib, R.H.; Rahman, M.M.; Asiri, A.M.; Siddiquey, I.A.; Islam, S.S.M.; Hasnat, M.A. Electrocatalytic oxidation of 4-aminophenol molecules at the surface of an FeS_2/carbon nanotube modified glassy carbon electrode in aqueous medium. *Chempluschem* **2019**, *84*, 175–182. [CrossRef] [PubMed]

39. Lazanas, A.C.; Prodromidis, M.I. Electrochemical Impedance Spectroscopy—A Tutorial. *ACS Meas. Sci. Au* **2023**, *3*, 162–193. [CrossRef] [PubMed]

40. Lasia, A. The Origin of the Constant Phase Element. *J. Phys. Chem. Lett.* **2022**, *13*, 580–589. [CrossRef] [PubMed]

41. Motin, M.A.; Uddin, M.A.; Dhar, P.K.; Mia, M.A.; Hashem, M.A. Study of Electrochemical Oxidation of Catechol in the Presence of Sulfanilic Acid at Different pH. *Port. Electrochimica Acta* **2017**, *35*, 103–116. [CrossRef]

42. Arpitha, S.B.; Swamy, B.E.K.; Banu, R. Electrochemical studies of catechol and hydroquinone at poly(nigrosine) modified carbon paste electrode: A cyclic voltammetric study. *Sens. Technol.* **2023**, *1*, 2258789. [CrossRef]

43. Manoj, D.; Gnanasekaran, L.; Rajendran, S.; Jalil, A.A.; Siddiqui, M.N.; Gracia, F.; So-to-Moscoso, M. A mechano-thermal ap-proach for the synthesis of Fe_3O_4 nanopar-ticles as dopant on mesoporous TiO_2 for elec-trochemical determination of catechol. *Environ. Res.* **2023**, *222*, 115358. [CrossRef]

44. Yu, J.; Du, W.; Zhao, F.; Zeng, B. High sensitive simultaneous determination of catechol and hydroquinone at mesoporous carbon CMK-3 electrode in comparison with multi-walled carbon nanotubes and Vulcan XC-72 carbon electrodes. *Electrochimica Acta* **2008**, *54*, 984–988. [CrossRef]

45. Alshahrani, L.A.; Li, X.; Luo, H.; Yang, L.; Wang, M.; Yan, S.; Liu, P.; Yang, Y.; Li, Q. The Simultaneous Electrochemical Detection of Catechol and Hydroquinone with [Cu(Sal-β-Ala)(3,5-DMPz)$_2$]/SWCNTs/GCE. *Sensors* **2014**, *14*, 22274–22284. [CrossRef] [PubMed]

46. Zhao, D.M.; Zhang, X.H.; Feng, L.J.; Jia, L.; Wang, S.F. Simultaneous determination of hydroquinone and catechol at PASA/MWNTs composite film modified glassy carbon electrode. *Colloids Surf. B Biointerfaces* **2009**, *74*, 317–321. [CrossRef]

47. Naik, T.S.K.N.; Swamy, B.E.K. Modification of carbon paste electrode by electrochemical polymerization of neutral red and its catalytic capability towards the simultaneous determination of catechol and hydroquinone: A voltammetric study. *J. Electroanal. Chem.* **2017**, *804*, 78–86. [CrossRef]

48. Feng, S.Q.; Zhang, Y.Y.; Zhong, Y.M. Simultaneous determination of hydroquinone and catechol using covalent layer-by-layer self-assembly of carboxylated-MWNTs. *J. Electroanal. Chem.* **2014**, *733*, 1–5. [CrossRef]

49. Li, M.; Ni, F.; Wang, Y.; Xu, S.; Zhang, D.; Chen, S.; Wang, L. Sensitive and Facile Determination of Catechol and Hydroquinone Simultaneously Under Coexistence of Resorcinol with a Zn/Al Layered Double Hydroxide Film Modified Glassy Carbon Electrode. *Electroanalysis* **2009**, *21*, 1521–1526. [CrossRef]

50. Hu, F.; Chen, S.; Wang, C.; Yuan, R.; Yuan, D.; Wang, C. Study on the application of reduced graphene oxide and multiwall carbon nanotubes hybrid materials for simultaneous determination of catechol, hydroquinone, p-cresol and nitrite. *Anal. Chim. Acta* **2012**, *724*, 40–46. [CrossRef]

51. Huo, Z.; Zhou, Y.; Liu, Q.; Liang, Y.; Xu, M. Sensitive simultaneous determination of catechol and hydroquinone using a gold electrode modified with carbon nanofibers and gold nanoparticles. *Microchim. Acta* **2011**, *173*, 119–125. [CrossRef]

52. Zhang, Y.; Sun, R.; Luo, B.; Wang, L. Boron-doped graphene as high performance electrocatalyst for the simultaneously electrochemical determination of hydroquinone and catechol. *Electrochim. Acta* **2015**, *156*, 228–234. [CrossRef]

53. Unnikrishnan, B.; Ru, P.L.; Chen, S.M. Electrochemically synthesized Pt–MnO_2 composite particles for simultaneous determination of catechol and hydroquinone. *Sens. Actuators B-Chem.* **2012**, *169*, 235. [CrossRef]

54. Wang, L.; Huang, P.; Bai, J.; Wang, H.; Zhang, L.; Zhao, Y. Direct simultaneous electrochemical determination of hydroquinone and catechol at a poly(glutamic acid) modified glassy carbon electrode. *Int. J. Electrochem. Sci.* **2007**, *2*, 123–132. [CrossRef]

55. Yang, P.; Zhu, Q.; Chen, Y.; Wang, F. Simultaneous determination of hydroquinone and catechol using poly(*p*-aminobenzoic acid) modified glassy carbon electrode. *J. Appl. Polym. Sci.* **2009**, *113*, 2881–2886. [CrossRef]

56. Erogul, S.; Bas, S.Z.; Ozmen, M.; Yildiz, S. A new electrochemical sensor based on Fe_3O_4 functionalized grapheme oxide-gold nanoparticle composite film for simultaneous determination of catechol and hydroquinone. *Electrochim. Acta* **2015**, *186*, 302–313. [CrossRef]

57. Saleem, Q.; Shahid, S.; Rahim, A.; Bajaber, M.A.; Mansoor, S.; Javed, M.; Iqbal, S.; Bahadur, A.; Aljazzar, S.O.; Pashameah, R.A.; et al. A highly explicit electrochemical biosensor for catechol detection in real samples based on copper-polypyrrole. *RSC Adv.* **2023**, *13*, 13443–13455. [CrossRef] [PubMed]

58. Bai, J.; Guo, L.; Ndamanisha, J.C.; Qi, B. Electrochemical properties and simultaneous determination of dihydroxybenzene isomers at ordered mesoporous carbon-modified electrode. *J. Appl. Electrochem.* **2009**, *39*, 2497–2503. [CrossRef]

59. Singh, R.P. A catechol biosensor based on a gold nanoparticles encapsulated-dendrimer. *Analyst* **2011**, *136*, 1216–1221. [CrossRef]